SUPPORTING INFORMATION

Nanoscale electrical excitation of surface plasmon polaritons with a nanoantenna tunneling junction

Authors: Delphine Pommier, Zélie Hufschmitt, Cheng Zhang, Yunhe Lai, Gérald Dujardin, Eric Le Moal, Christophe Sauvan, Jean-Jacques Greffet, Jianfang Wang, and Elizabeth Boer-Duchemin

15 pages, 9 figures

Supporting information: Nanoscale electrical excitation of surface plasmon polaritons with a nanoantenna tunneling junction

Delphine Pommier,[†,§] Zélie Hufschmitt,[†] Cheng Zhang,[‡] Yunhe Lai,[¶] Gérald Dujardin,[†] Eric Le Moal,[†] Christophe Sauvan,[‡] Jean-Jacques Greffet,[‡] Jianfang Wang,[¶] and Elizabeth Boer-Duchemin[*,†]

†*Institut des Sciences Moléculaires d'Orsay (ISMO), CNRS, Université Paris-Saclay, Orsay (France)*

‡*Laboratoire Charles Fabry, Institut d'Optique Graduate School, CNRS, Université Paris-Saclay, Palaiseau (France)*

¶*Department of Physics, The Chinese University of Hong Kong, Shatin, Hong Kong SAR, (China)*

§*Present address: Thales Research and Technology, Palaiseau (France)*

E-mail: Elizabeth.Boer-Duchemin@universite-paris-saclay.fr

S1 Characterization of the thin Au film with and without the molecular layer

The sample studied in this article is a gold nanocube separated from a 50-nm Au film on glass by a ∼1 nm insulating layer of 1,8-octanedithiol (C8DT) molecules. The gold film is deposited by evaporation on a glass coverslip (5-nm Ti adhesion layer). In this section, the

gold film with and without the molecular layer is studied by atomic force microscopy (AFM) and optical transmission spectroscopy. Figure S1 shows the AFM results: the film is shown to have the same roughness with and without the molecules to within experimental error. In Figure S2, the optical transmission spectra of the gold film with and without the C8DT layer are shown. Any differences between the two curves are within the experimental error, suggesting that the absorption of light by the dithiol layer is negligible.

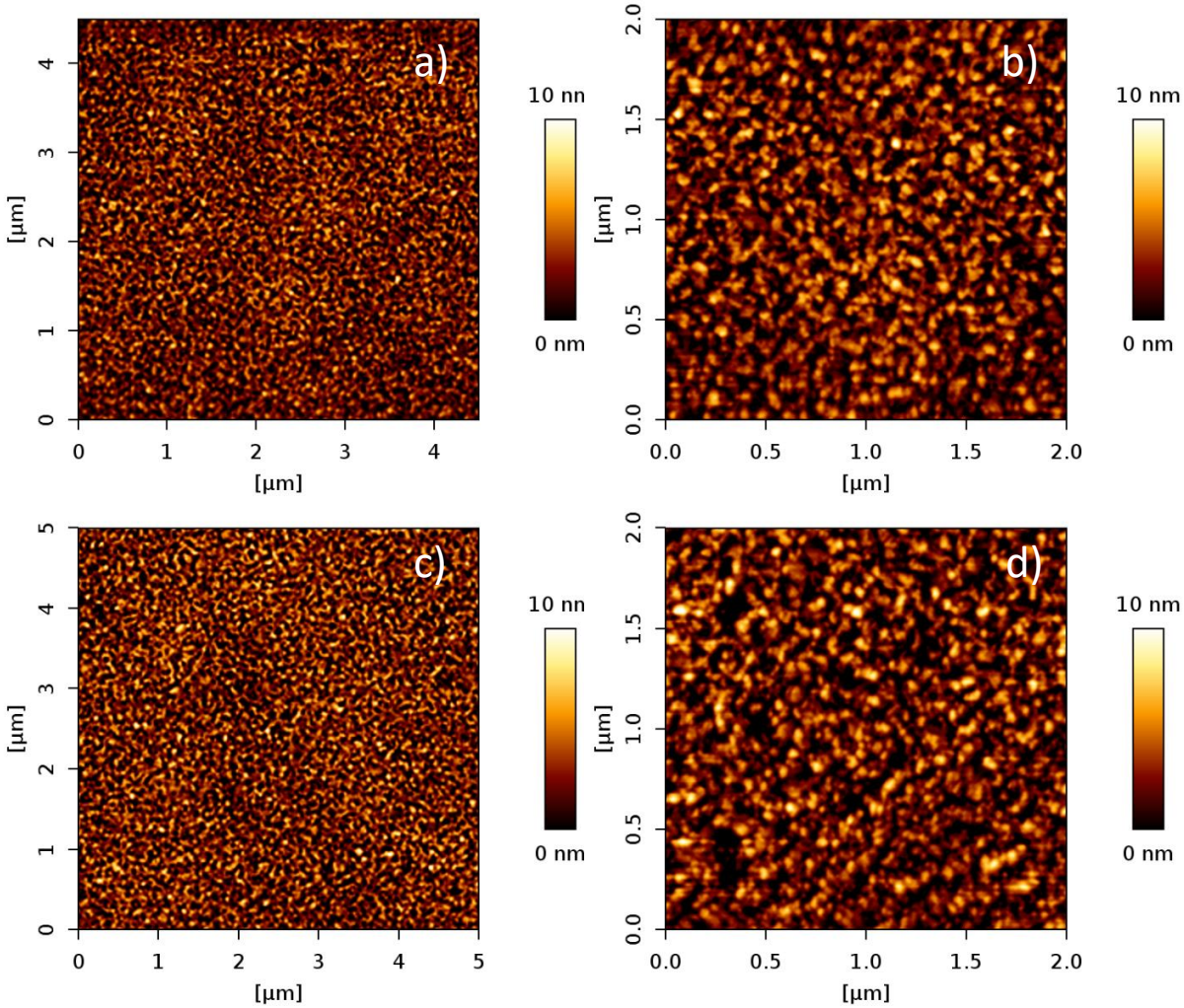

Figure S1: Atomic force microscopy of a gold film with and without molecular functionalization. a) and b) AFM of the bare Au film (root-mean-square roughness 2.12±0.03 nm). c) and d) AFM of the Au film functionalized by 1,8-octanedithiol molecules. In this case the RMS-roughness is 2.10±0.03 nm.

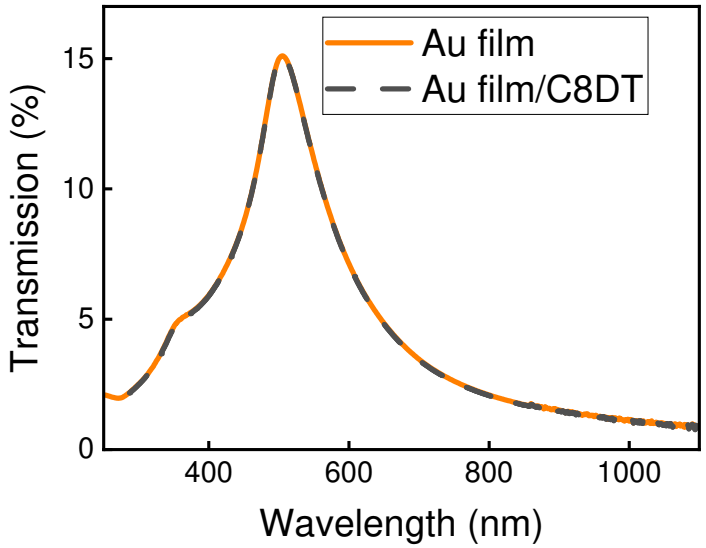

Figure S2: Optical transmission measurements of a gold film with and without molecular functionalization. Any differences between the curves are within the experimental error.

S2 Fourier plane analysis

Figure S3 a) shows the result when twenty-two cross-sections from Fig. 2 b) of the main text are averaged. Panels b) and c) of Fig. S3 show enlarged versions of the peaks. Note that due to the limited resolution of the Fourier plane image, there are only four pixels in each peak at intensity values higher than the half maximum. Note also the small shoulder visible at higher values of $|\frac{k_{||}}{k_0}|$, suggesting that multiple peaks are present. Indeed, a broader (or narrower) spectrum should give rise to broader (or narrower) peaks in the Fourier plane cross-sections; however, this is difficult to evaluate in the present case given the resolution of our Fourier plane images. In order to determine the central value of a peak, a simple Gaussian fit was used since using a multiple peak fit was unsatisfactory (poor convergence). The resulting measured $\frac{k_{||}}{k_0}$ value is 1.025±0.009.

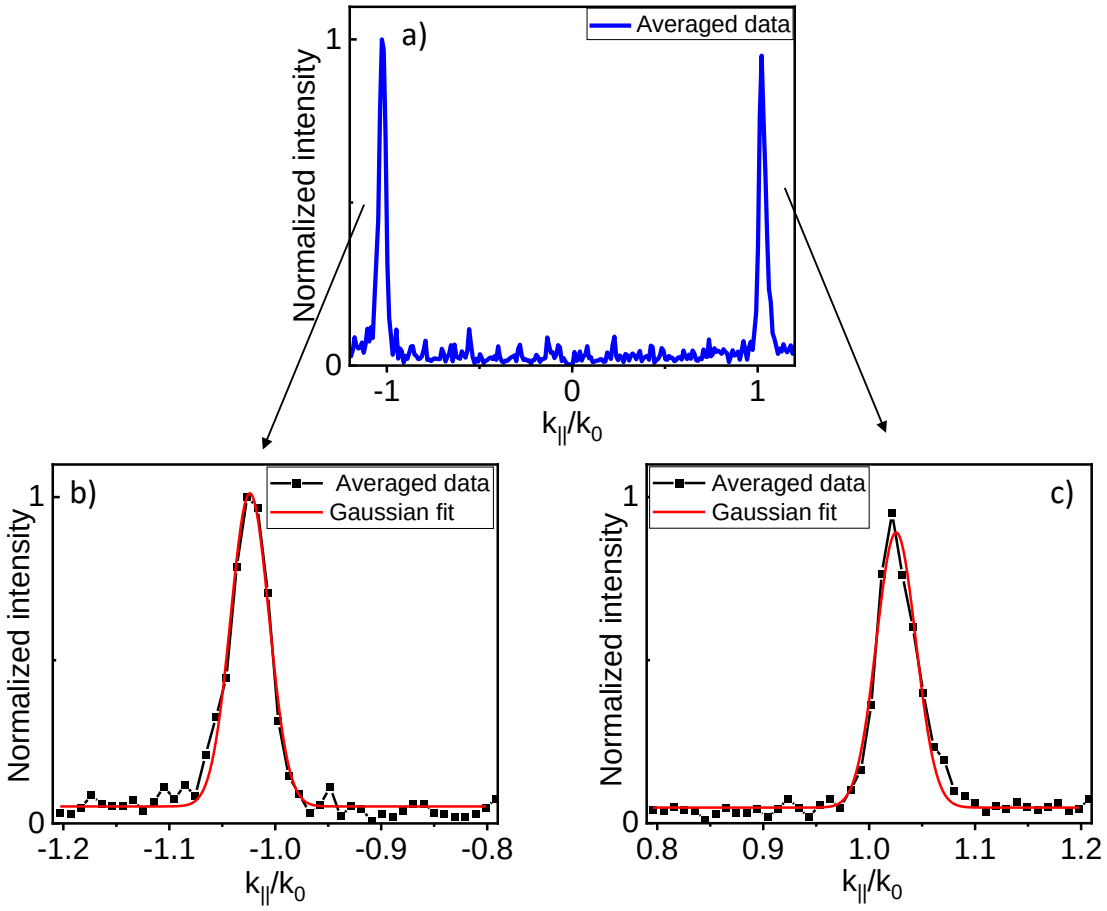

Figure S3: Averaged cross-section from the Fourier plane image. a) Result after the averaging of twenty-two cross-sections from Fig. 2 b) of the main text. b) and c) Enlargements of panel a) showing the pixel size and the Gaussian fits to the data.

S3 Simulation of the emission from a tunneling junction in a "nanoantenna-on-a mirror" geometry

In order to calculate the spectrum of the light emitted from the "nanoantenna-on-a-mirror" system, we use a full-wave electromagnetic solver.[1,2] The nanocube is approximated as a cylinder with an aspect ratio of 1, i.e., the height and diameter of the cylinder are equal, and the molecular film is considered a dielectric with an index of refraction of 1.5. The inelastic tunneling current is modeled as a vertical oscillating point dipole in the center of the junction[3] (see Fig. S4).

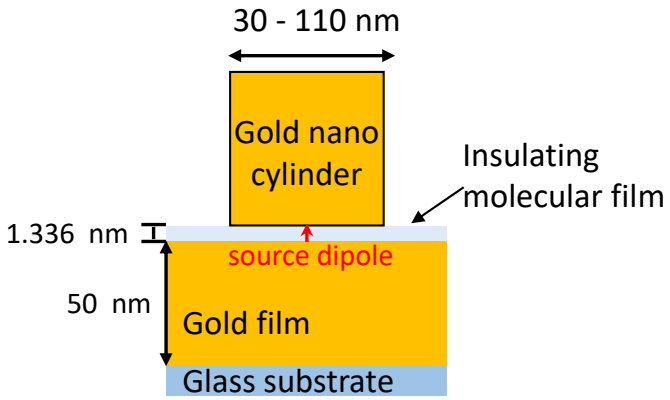

Figure S4: System used in the numerical calculations: gold nanocylinder on a gold film functionalized by insulating molecules.

A nanoscale plasmonic system possesses eigenmodes of different specific frequencies and field or charge distributions. The type of system studied (often called a nanoparticle-on-a-mirror, or a metal-insulator-metal nanoresonator) has both *longitudinal* plasmonic *nanoantenna* modes involving oscillating charges in the structure and image charges in the substrate, and *transverse* plasmonic *gap* modes supported in the insulating layer gap and reflecting on the edges of the cylinder.[4,5] In the following, we denote the gap modes as S_{mn} and the longitudinal nanoantenna modes as L_{mn} following the notation used in Refs. [1, 4], with n being the mode order and m the azimuthal number. Here the mode order n corresponds to the number of nodes in the vertical electric field below the antenna. Thanks to the symme-

try of revolution of the system used in the calculation (the cubic antenna is modeled as a cylinder), we decompose the electromagnetic field in a sum of azimuthal eigenmodes where for each mode the electromagnetic field varies as $e^{im\theta}$ with θ the angle in the plane of the film (as usually defined in cylindrical coordinates) and m the azimuthal number. Note that hybridization between two modes is only possible if they have the same azimuthal number.[1] Moreover, only modes with the azimuthal number $m = 0$ may be excited by a vertical point dipole source on the antenna axis. This selection rule is a limitation of the model (see Section S4 below for further discussion).

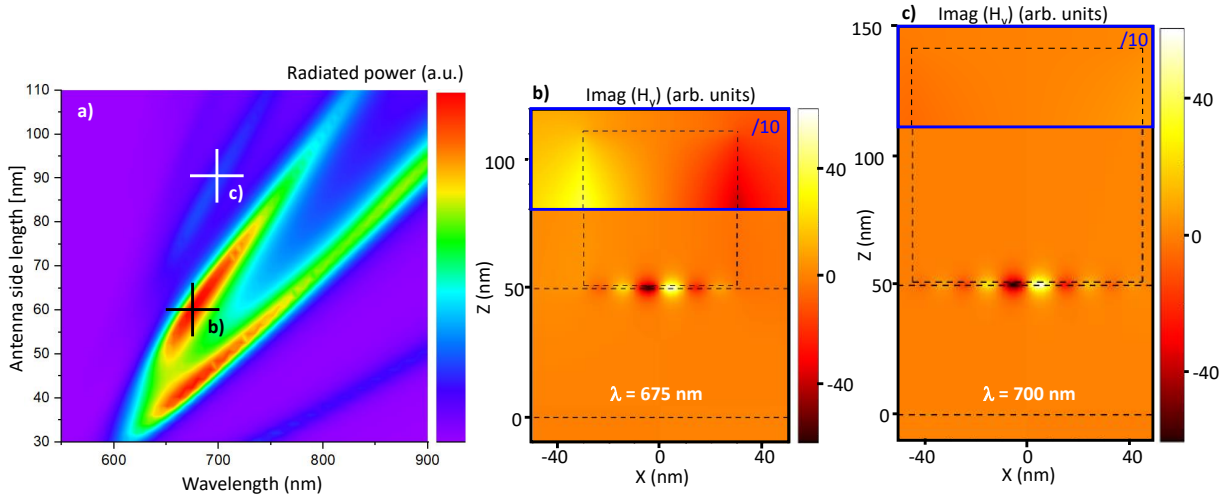

Figure S5: Calculated radiated power as a function of antenna side length and emission wavelength, and mode magnetic field distributions. a) The calculated power radiated below the substrate in the collection angle of the objective lens is plotted as a function of antenna side length and emission wavelength. This figure is a reproduction of Fig. 4 a) in the main text. b) Magnetic field distribution in a plane perpendicular to the substrate calculated for the corresponding point shown in part a), i.e., side length 60 nm, wavelength 675 nm. The dashed black lines in b) represent the position of the antenna and the gold film. An intense field is seen in the region between the antenna and the film, and is attributed to a gap mode. Plotting the area enclosed in the blue rectangle using a colour scale reduced by a factor of 10, we demonstrate the existence of an antenna mode (field on the sides of the nanoantenna, see Fig. S7). c) Same as for part b), but for an antenna of side length 90 nm and at a wavelength of 700 nm. In this case, no evidence of an antenna mode is found when the colour scale is reduced for the upper part of the graph.

Figure S5 a) again displays the data of Fig. 4 a) of the main text. Parts b) and c), however, show the calculated magnetic field distributions for *different* antenna side lengths

and emission wavelengths as opposed to what is shown in Fig. 4 (see the crosses in part a)). Looking at the number of nodes in the magnetic field in the gap in the data presented here we can conclude the following: the "faint" line seen in the top left section of part a) corresponds to the gap mode S_{010} (see Fig. S5 c)) and no indication of an antenna mode is detected (see the upper region of Fig. S5 c)). Figure S5 b) shows that the *intense* line in part a) corresponds to the S_{06} gap mode; most importantly, in this case, the hybridization with an antenna mode is clear (see the upper region of Fig. S5 b)). Thus the lines from part a) correspond to a particular gap mode, whose wavelength increases with increasing side length, as would be expected.[6] The supplementary data here supports the conclusion that the enhancement of the emission seen for antenna side lengths and wavelengths determined from the intense lines in part a) may be attributed to the coupling between the gap modes and the antenna mode L_{01}. When the gap and antenna modes couple, we could expect to see an anti-crossing of the modes due to strong coupling. However, due to large mode widths and small coupling strengths (and thus small differences in energy between the hybridized modes), no evidence of strong coupling is observed.[1]

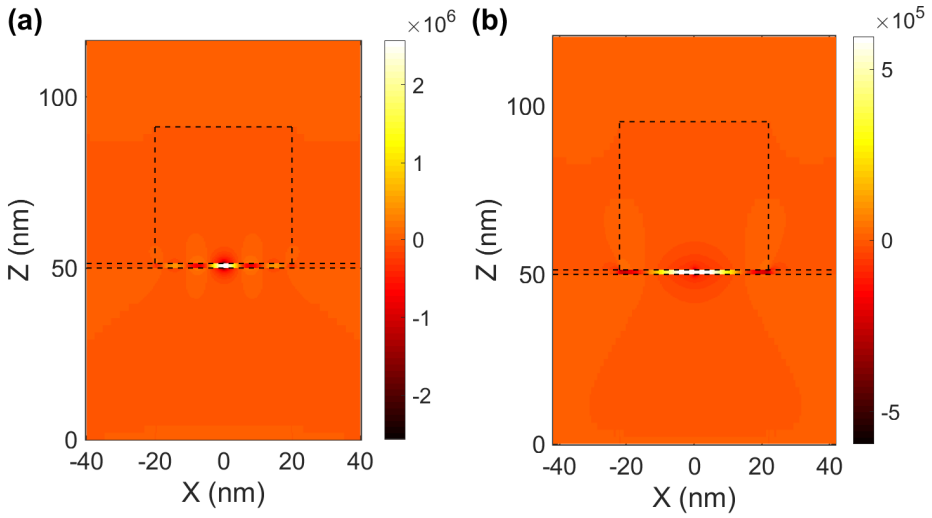

Figure S6: Calculation of the imaginary part of the y-component of the electric field for a nanoantenna of the same side lengths and at the same wavelengths as for the magnetic field calculations in Fig. 4 d) and e) of the main text, i.e., a) $\lambda = 660$ nm and b) $\lambda = 850$ nm. Note the difficulty of identifying the modes at play due to the intense electric field in the gap region. The units for the electric field are arbitrary and the scale is linear.

Figure S6 shows the electric field distributions for a nanoantenna of the same side lengths and at the same wavelengths as for the magnetic field calculations in Fig. 4 d) and e) of the main text (i.e., $\lambda = 660$ nm for part a) and $\lambda = 850$ nm for part b).) Note the very intense electric field in the gap region. Since we model the light emission from inelastic tunneling as a point source, the electric field can be understood as the superposition of three contributions: the field of the excited mode(s) weighted by an excitation coefficient, a field that is extremely intense around the metal interfaces close to the source (this field is responsible for the quenching phenomenon), and a singularity at the source position (due to the singularity of the real part of the Green tensor).[7] Plotting the imaginary part of the field allows us to suppress the singularity. However, even without the singularity of the Green tensor, the modal contribution is hidden by the intense field responsible for quenching. This quenching contribution, however, is much less intense in the magnetic field. This is why we choose to show the magnetic field in the main text. Plotting the magnetic field allows us to more easily identify the modes that are excited by the tunneling current.

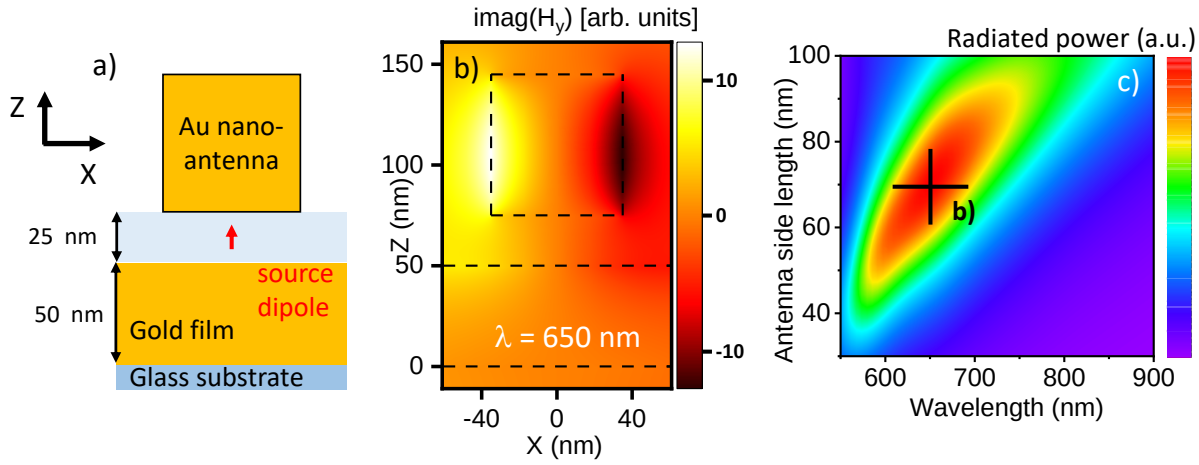

Figure S7: The antenna mode. a) Sketch of the system used in the calculations. b) Calculated magnetic field distribution ($Im(H_y)$) for an antenna with side length 70 nm, and gap thickness 25 nm, at an emission wavelength of 650 nm. For these parameters, the antenna mode dominates, and the imaginary part of the magnetic field in the direction perpendicular to the page is strongest along the sides of the antenna. c) Calculated radiated power as a function of antenna side length and wavelength. The color scale is linear and is in arbitrary units. The black cross denotes the antenna size and wavelength used in the calculations of the field in part b).

In Fig. S7, we explore the antenna mode of the nanocube antenna. To do so, we increase the gap thickness to 25 nm (see Fig. S7 a)). Note that while this weakens the gap mode, the coupling of the oscillating charge in the nanoantenna to its image charge in the substrate is also reduced. In panel b) of Fig. S7 the result of the calculation for the magnetic field distribution ($Im(H_y)$) when the antenna side length is 70 nm and the wavelength is 650 nm may be seen. We see that when these particular parameters are chosen the antenna mode dominates. This is demonstrated by the high intensity of the imaginary part of the magnetic field on the sides of the nanoantenna. In panel c) of the figure, the radiated power as a function of antenna side length and wavelength is plotted. Since the side length is the same as the height of the antenna (since it is a cube), the resonance shifts to longer wavelengths with increasing side length as would be expected. Note that while this same tendency is expected for all gap thicknesses, the exact position of the resonance varies with the distance of the antenna to the film.

S4 Approximations used in the model and additional experimental spectra

As is generally the case, the system has been simplified so that calculations may be more easily carried out. In particular, the code has been developed for systems with axial symmetry, meaning that in fact the cubic nanoantenna with rounded edges is represented by a cylinder with sharp edges whose height and diameter are equal. Thus, clearly the available modes in the experimental and theoretical systems will not be identical.[4,8] These are some of the reasons why the experimental and simulated results are not identical in the additional data shown Fig. S8. Another important approximation is the fact that the tunneling current is represented by a single oscillating vertical electric dipole in the center of the system, while in reality the tunneling current flows throughout the junction—in other words, the entire gap should be filled with dipole sources along the horizontal direction. The result of this

approximation is that certain modes are not excited theoretically due to symmetry considerations (see Section S3 above), while experimentally these modes may participate in the emission. The calculations also ignore the presence of the platinum atomic force microscope tip. The presence of a nonplasmonic tip is expected to add loss channels, but is not thought to alter the lower order antenna modes significantly.[9,10] Thus, neglecting or underestimating the losses of the material parameters may be another reason for the disagreement between the experiments and simulations, leading to broader experimental peaks as compared to the simulated results (see for example panel c) of Fig. S8). Platinum is technically a plasmonic material in the wavelength range of interest (i.e., the real part of the metal dielectric function is negative), but its losses are relatively high.[11] Thus the tip may increase the effective height of the nanoantenna and redshift the experimental spectrum in comparison to the simplified calculation (see for example panel b) of Fig. S8). Finally, the gold film is considered perfectly flat in the model, which is clearly not the case experimentally (see Fig. S1). Such roughness could lead to the formation of "picocavities" which have been shown to play an important role in the optical response at the nanoscale.[12,13] The roughness of the film also leads to local variations in the antenna gap thickness. The influence of the gap thickness on the calculated spectrum is explored further in the following section.

Figure S8 shows the spectra obtained from experiments on nanoantennas of different sizes. The corresponding simulated curves are the appropriate cross-sections from Fig. 4 a) of the main text. We see indeed that the antenna side length influences the spectrum, with the reasons for the discrepancies between experiment and theory described above. Note that in the literature, samples consisting of molecules deposited on substrates have been excited using the tunneling current between the tip of a scanning tunneling microscope and the sample, leading to the emission of light (consider for example Ref. 14). These experiments have been carried out in ultrahigh vacuum and at low temperature. This light emission is usually attributed to the recombination of an electron and hole, with the spectrum reflecting the different energy levels of the molecule. Even without considering the electronic structure

of the molecules used here (1,8-octanedithiols), we can rule out this phenomenon in our case by comparing the results of Fig. S8 a) and c); if the resonances in the spectra were due to the molecules, the shift of $\sim$ 100 nm seen in the spectra shown in parts a) and c) of the figure would not be present. This is thus further evidence that the resonances seen in the measured spectra are due to the nanoantenna modes of the sample.

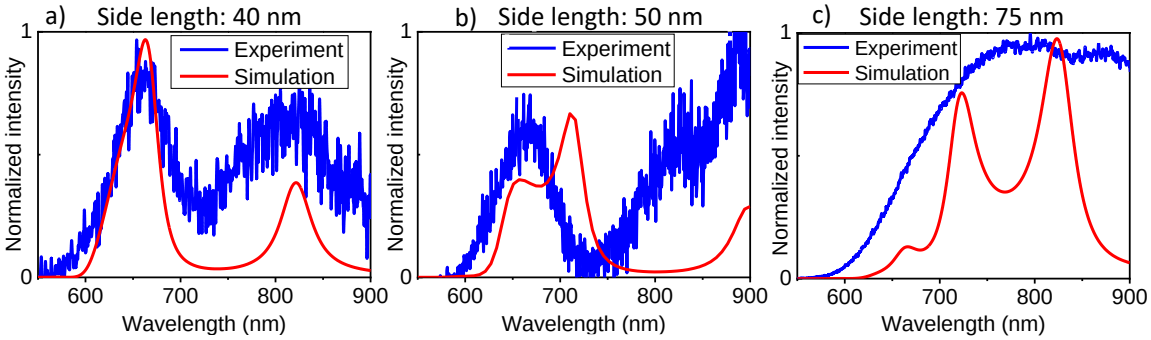

Figure S8: Experimental and simulated spectra for different nanoantenna side lengths. Results for side lengths of a) 40, b) 50 and c) 75 nm. Note that part a) is the same data as Fig. 4 of the main text, reproduced here for comparison purposes. While the normalization for parts a) and c) is carried with respect to the maximum values of the respective curves, the data in part b) is normalized with respect to the peak at $\sim$ 650 nm.

S5 Dependence of the emission spectrum on the gap thickness

In order to estimate the impact of the gap thickness, the spectrum of the emitted light as a function of the gap thickness is plotted in Fig. S9 for a 50-nm nanocube. Using the same strategy as in Fig. S5 above, we plot the transverse magnetic field in order to identify the modes at play. Here the S_{04}, S_{06} and S_{08} gap modes may be identified. The gap mode resonances are seen to blue shift with increasing gap thickness: when the gap thickness increases, the effective index of the gap plasmon decreases, which blue shifts the gap mode.[15] Note that the antenna mode is less sensitive to the gap-thickness variation as compared to the gap mode. As in the main text, the increase in the power radiated into the far field at

the wavelength of ~ 675 nm is attributed to the coupling between the antenna mode and the gap modes. Thus, we see that a small variation of the gap thickness can significantly shift the resonances in the simulated spectrum; for example, a change in the thickness of the gap from 0.9 nm to 1.05 nm gives rise to a shift on the order of ~ 40 nm for the dominant peak of the spectrum. Thus, imprecise knowledge of the thickness of the gap may be a source of discrepancy between the experimental data and the simulations.

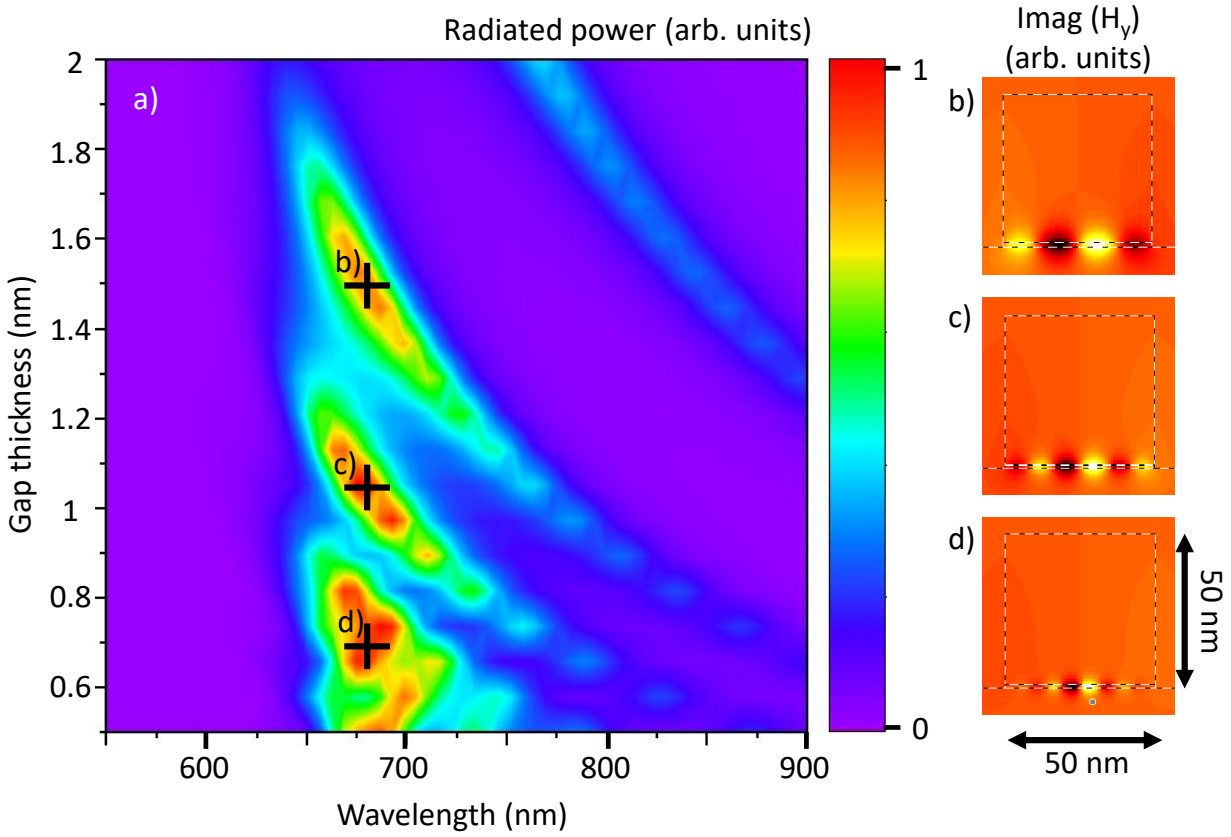

Figure S9: Calculated radiated power into the far-field as a function of gap thickness. a) The calculated power radiated below the substrate in the collection angle of the objective lens is plotted as a function of gap thickness and wavelength. Four resonant branches are seen which blue shift as the gap thickness increases. b), c) and d) Magnetic field distributions in a plane perpendicular to the substrate calculated for the corresponding gap thicknesses and wavelengths marked by black crosses in part a). The dashed black and white lines delineate the antenna and the gold film. An intense field is seen in the region between the antenna and the gold film and is attributed to the gap modes b) S_{04}, c) S_{06}, and d) S_{08} respectively.

Note also that below a gap thickness of ~ 1 nm, quantum mechanical effects begin to play a role in the electromagnetic results. These effects include nonlocal charge screening

and electron spill-out, and the emergence of charge transfer plasmon modes, which lead to blue-shifted resonances.[16–21] Nanoantenna junctions with smaller gaps than those considered here must take into account these effects.

References

(1) Zhang, C.; Hugonin, J.-P.; Greffet, J.-J.; Sauvan, C. Surface Plasmon Polaritons Emission with Nanopatch Antennas: Enhancement by Means of Mode Hybridization. *ACS Photonics* **2019**, *6*, 2788–2796.

(2) Bigourdan, F.; Hugonin, J.-P.; Lalanne, P. Aperiodic-Fourier modal method for analysis of body-of-revolution photonic structures. *J. Opt. Soc. Am. A* **2014**, *31*, 1303–1311.

(3) Johansson, P. Light emission from a scanning tunneling microscope: Fully retarded calculation. *Phys. Rev. B* **1998**, *58*, 10823–10834.

(4) Tserkezis, C.; Esteban, R.; Sigle, D. O.; Mertens, J.; Herrmann, L. O.; Baumberg, J. J.; Aizpurua, J. Hybridization of plasmonic antenna and cavity modes: Extreme optics of nanoparticle-on-mirror nanogaps. *Phys. Rev. A* **2015**, *92*, 053811.

(5) Choo, H.; Kim, M.-K.; Staffaroni, M.; Seok, T. J.; Bokor, J.; Cabrini, S.; Schuck, P. J.; Wu, M. C.; Yablonovitch, E. Nanofocusing in a metal–insulator–metal gap plasmon waveguide with a three-dimensional linear taper. *Nature Photonics* **2012**, *6*, 838–844.

(6) Qian, H.; Hsu, S.-W.; Gurunatha, K.; Riley, C. T.; Zhao, J.; Lu, D.; Tao, A. R.; Liu, Z. Efficient light generation from enhanced inelastic electron tunnelling. *Nature Photonics* **2018**, *12*, 485–488.

(7) Yan, W.; Faggiani, R.; Lalanne, P. Rigorous modal analysis of plasmonic nanoresonators. *Phys. Rev. B* **2018**, *97*, 205422.

(8) Faggiani, R.; Yang, J.; Lalanne, P. Quenching, Plasmonic, and Radiative Decays in Nanogap Emitting Devices. *ACS Photonics* **2015**, *2*, 1739–1744.

(9) Le Moal, E.; Marguet, S.; Rogez, B.; Mukherjee, S.; Dos Santos, P.; Boer-Duchemin, E.; Comtet, G.; Dujardin, G. An Electrically Excited Nanoscale Light Source with Active Angular Control of the Emitted Light. *Nano Lett.* **2013**, *13*, 4198–4205.

(10) Le Moal, E.; Marguet, S.; Canneson, D.; Rogez, B.; Boer-Duchemin, E.; Dujardin, G.; Teperik, T. V.; Marinica, D.-C.; Borisov, A. G. Engineering the emission of light from a scanning tunneling microscope using the plasmonic modes of a nanoparticle. *Phys. Rev. B* **2016**, *93*, 035418.

(11) Palik, E. D., Ed. *Handbook of optical constants of solids III*; Academic Press: New York, 1998.

(12) Yang, B.; Chen, G.; Ghafoor, A.; Zhang, Y.; Zhang, Y.; Zhang, Y.; Luo, Y.; Yang, J.; Sandoghdar, V.; Aizpurua, J.; Dong, Z.; Hou, J. G. Sub-nanometre resolution in single-molecule photoluminescence imaging. *Nature Photonics* **2020**, *14*, 693–699.

(13) Wu, T.; Yan, W.; Lalanne, P. Bright Plasmons with Cubic Nanometer Mode Volumes through Mode Hybridization. *ACS Photonics* **2021**, *8*, 307–314.

(14) Dong, Z. C.; Zhang, X. L.; Gao, H. Y.; Luo, Y.; Zhang, C.; Chen, L. G.; Zhang, R.; Tao, X.; Zhang, Y.; Yang, J. L.; Hou, J. G. Generation of molecular hot electroluminescence by resonant nanocavity plasmons. *Nature Photonics* **2010**, *4*, 50–54.

(15) Romero, I.; Aizpurua, J.; Bryant, G. W.; Abajo, F. J. G. d. Plasmons in nearly touching metallic nanoparticles: singular response in the limit of touching dimers. *Opt. Express* **2006**, *14*, 9988–9999.

(16) Savage, K. J.; Hawkeye, M. M.; Esteban, R.; Borisov, A. G.; Aizpurua, J.; Baum-

berg, J. J. Revealing the quantum regime in tunnelling plasmonics. *Nature* **2012**, *491*, 574–577.

(17) Esteban, R.; Borisov, A. G.; Nordlander, P.; Aizpurua, J. Bridging quantum and classical plasmonics with a quantum-corrected model. *Nat Commun* **2012**, *3*, 825.

(18) Teperik, T. V.; Nordlander, P.; Aizpurua, J.; Borisov, A. G. Robust Subnanometric Plasmon Ruler by Rescaling of the Nonlocal Optical Response. *Phys. Rev. Lett.* **2013**, *110*.

(19) Benz, F.; Tserkezis, C.; Herrmann, L. O.; de Nijs, B.; Sanders, A.; Sigle, D. O.; Pukenas, L.; Evans, S. D.; Aizpurua, J.; Baumberg, J. J. Nanooptics of Molecular-Shunted Plasmonic Nanojunctions. *Nano Lett.* **2015**, *15*, 669–674.

(20) Zhu, W.; Esteban, R.; Borisov, A. G.; Baumberg, J. J.; Nordlander, P.; Lezec, H. J.; Aizpurua, J.; Crozier, K. B. Quantum mechanical effects in plasmonic structures with subnanometre gaps. *Nat Commun* **2016**, *7*, 11495.

(21) Cui, X.; Qin, F.; Lai, Y.; Wang, H.; Shao, L.; Chen, H.; Wang, J.; Lin, H.-q. Molecular Tunnel Junction-Controlled High-Order Charge Transfer Plasmon and Fano Resonances. *ACS Nano* **2018**, *12*, 12541–12550.